Advances in Geological and Geotechnical Engineering Research
https://ojs.bilpublishing.com/index.php/agger

ARTICLE

Source Area Weathering and Tectonic History Inferred from the Geochemistry of the Maastrichtian Sandstone from Patti Formation, Southern Bida Basin, North Central Nigeria

R. G. Oladimeji[1*] O. J. Ojo[2]

1. Department of Geological Sciences, Osun State University, Osogbo, Osun State, Nigeria
2. Department of Geology, Federal University, Oye Ekiti State, Nigeria

ARTICLE INFO

Article history
Received: 29 July 2022
Revised: 08 September 2022
Accepted: 14 September 2022
Published Online: 27 September 2022

Keywords:
Patti formation sandstone
Chemical weathering
Passive margin
Continental drift
Climatic condition

ABSTRACT

Sandstones sampled from Patti Formation, Southern Bida Basin, were studied geochemically using Inductively Coupled Plasma Atomic Emission Spectrophotometer (ICP-AES) and an Inductively Coupled Plasma Mass Spectrometry (ICP-MS) technique to evaluate their weathering and tectonic setting as well as to deduce the paleo-climatic conditions that existed during their deposition. Geochemically, SiO_2 range from 73.9% to 86.2%, Al_2O_3 (6.7%~17.1%), Fe_2O_3 (1.1%~1.9%), K_2O (0.1%~0.7%) while MgO, CaO, Na_2O, P_2O_5, MnO and TiO_2 were <1%. Enriched in Ba (Av. 622.94), Sr (Av. 153.63), Rb (Av. 55.08) and Zr (Av. 51.86) relatively similar in composition to UCC. High SiO_2 but low other major oxides signify high mobility during processes of weathering. This was confirmed by high value (>80%) for indices like chemical index of alteration, chemical index of weathering, plagioclase index of alteration, mineralogical index of alteration and relatively lower values for weathering index of parker, recently used alpha indices ($\alpha^{Al}{}_{E}$) of sodium ($326.17\alpha^{Al}{}_{Na}<344.40$), magnesium ($100.54\alpha^{Al}{}_{mg}<398.55$), calcium ($12.07\alpha^{Al}{}_{Ca}<198.99$), potassium ($4.43\alpha^{Al}{}_{K}<64.33$), strontium ($0.84\alpha^{Al}{}_{E}<21.40$), barium ($0.45\ \alpha^{Al}{}_{Ba}<10.52$) and rubidium ($0.0008\alpha^{Al}{}_{Rb}<0.06$), supported by AI_2O_3-(CaO^*+Na_2O)-K_2O and CIA vs. SiO_2 plots that imply intense weathering in the source area. The obtained high CIA values (>80) indicates a steady-state of weathering under a warm/humid climate as confirmed by the SiO_2 vs. Al_2O_3+ K_2O + Na_2O plot. High average SiO_2 (75.41wt%) with K_2O/Na_2O ratio >1 (15.63), low Fe_2O_3 (1.27wt %), Al_2O_3 (15.82wt%) and TiO_2 (0.46) suggest passive margin tectonic setting. This is supported by enriched ΣREE (209.64 ppm), ΣLREE (195.78), LREE/HREE (27.78) and negative Eu/Eu* (0.68), plots of log (K_2O/Na_2O) vs. SiO_2 and SiO_2/Al_2O_3 vs. K_2O/Na_2O. Major elements discriminant-function multi-dimensional diagram, DF1 (arc-rift-col) vs. DF2 (arc-rift-col), for high-silica sediments revealed a continental rift tectonic setting. Thus, the Patti Formation sandstone underwent a high degree of weathering under a humid climatic condition within a continental rift tectonic setting.

*Corresponding Author:
R. G. Oladimeji
Department of Geological Sciences, Osun State University, Osogbo, Osun State, Nigeria;
Email: oladi21may@yahoo.com

DOI: https://doi.org/10.30564/agger.v4i3.4933

1. Introduction

The Mid-Niger Basin, also known as the Bida Basin or the Nupe Basin, is a structurally depressed shape flanking the Sokoto and Anambra Basins, situated in Northcentral Nigeria. It is classified as an intracratonic basin that trends in a northwest- southeast direction. (Figure 1a; Figure 2) [1-3].

Geographically, the Bida Basin is sub-divided into Northern Bida Basin (NBB) and Southern Bida Basin (SBB) with a sedimentary fill of about 4 km, active during Campanian-Maastrichtian period in Nigeria [4,2] (Figure 1b). The Maastrichtian Patti Formation is sandwiched in between the basal Campanian Lokoja and the youngest Agbaja Formations, part of the southern Bida Basin [5] (Figure1b; Figure 2).

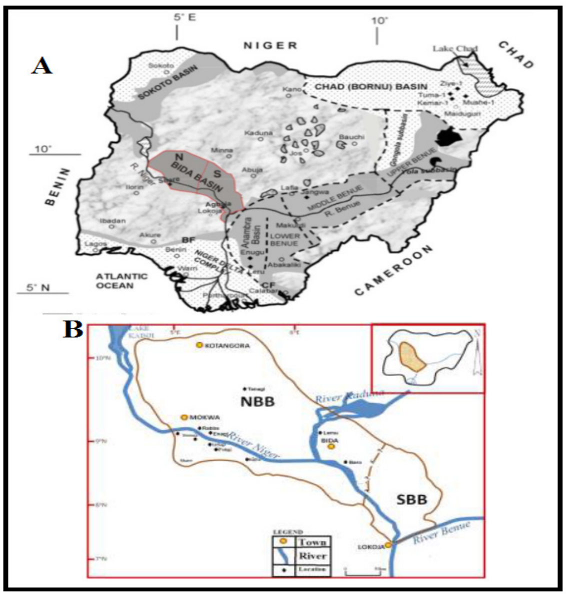

Figure 1. Map of **A**: Nigeria showing location of the Bida Basin [6] and **B**: Geographical division of the Bida Basin [7,6,2]

AGE	NORTHERN BIDA BASIN		SOUTHERN BIDA BASIN		DEPOSITIONAL ENVIRONMENT
MAASTRICHTIAN	Batati Formation		Agbaja Formation		Continental-Shallow marine
	Enagi Formation		Patti Formation		Brackish-Shallow marine
	Sakpe Formation				
CAMPANIAN	Bida Formation	Jima Member	Lokoja Formation	Claystone (member)	Continental Fluvial Deposits
				Sandstone (member)	
		Doko Member		Basal Conglomerate (member)	
					Unconformity
PRE-LOWER PALEOZOIC					Basement Complex

Figure 2. Regional stratigraphic successions in the Bida Basin [8].

In addition, although not limited to Falconer [9], Jones [7], Adeleye [10], Jan du Chene et al. [11], Agyingi [12], Braide [4], Ladipo et al. [13], Abimbola [14], Obaje et al. [6]; Udensi and Osasuwa [2]; Akande et al. [15]; Ojo and Akande [8]; Nton and Adamolekun [16]; Odundun and Ogundoro [3]; Ojo et al. [17] focused on the geology, stratigraphy, sedimentology, mineralogy and hydrocarbon potential of the different formations within the basin with paucity of information on the geochemistry of the basin most especially the Patti Formation, Southern Bida Basin to deduce its source area weathering and tectonic setting.

Ojo and Akande [18] documented facies correlation and depositional settings for the Upper Cretaceous Lokoja Formation while Ojo and Akande [19] reported on the sedimentology and depositional environment of the Patti Formation within the Bida Basin, focusing their study majorly on the field relationship, textural and palaeocurrent characteristic.

Signatures of geochemical compositions in sediments gives the nature and proportion of their detrital components that can lead to source area weathering, tectonic setting, climate and provenance determination as established by Bhatia [20]; McLennan et al. [21]; Armstrong-Altrin et al. [22]; Dey et al. [23]; Maharana et al. [24]; Tang et al. [25]; Ayala-Perez et al. [26]. This because, according to Bhatia [20]; Roser and Korsch [27]; McLennan et al. [21], chemical composition of clastic sedimentary rocks depend on numerous variables such as: nature of source rocks, source area weathering and diagenesis. More also, within a sedimentary basin, tectonic setting can be considered as the major control on the composition of sedimentary rocks as different tectonic setting have distinctive process of sedimentation and characteristic parent rocks/precursors [28,29].

Siliciclastic deposits can be regarded as excellent records for past environmental settings [30,31]. That can provide information principally appropriate for the re-construction of climatic conditions. Viers et al. [32], put forward that the fact that most fine-grained sediment carried in suspension is eroded soil derived from the source areas whose mineralogy and geochemistry, namely the levels of depletion in mobile elements relative to parent rocks, are largely dependent on weathering intensity suggest a link between fluvial mud composition and climate. In addition, rate of weathering has a vital role in response to mechanisms of the system of climate making its investigations particularly petinent [30].

The current study is focused on the application of geochemical signatures to unravel the source area weathering, tectonic setting with paleoclimatic history of sandstones from Patti Formation, Southern Bida Basin. This study gives an enhanced understanding of the area, particularly from a geochemical perception, while taking into consideration the discriminative compatibility of various weathering and tectonic indices and plots.

2. Location of Study Area and Stratigraphy of Southern Bida Basin

The area of study is part of Southern Bida Basin (Lokoja–Abaji–Abuja; Figures 1a and 1b) and falls within Federal Capital Territory and Kogi State. It covers parts of 1:50,000 Sheets 247 Lokoja (NE and NW), 227 Koton Karfi (NE and SE) and 206 Kwali (SE) (Figure 1). Bida Basin is an intracratonic basin that stretches northwest - southeast for about 400Km from Kontagora in Niger State to Dekina in Kogi State where it merged with the Anambra Basin. The basin has a maximum width of about 160 km (Figure 3).

Patti Formation

Patti Formation, which is our focus, directly overlies the Lokoja Formation and consists predominantly of siltstone, claystone, sandstone and shales inter bedded with bioturbated ironstones (Figures 1a and 1b; Figure 2). It is lateral equivalent of Enagi siltstone in the Northern Bida Basin. The Patti Formation is well exposed around Ahoko and Abaji. Argillaceous units predominate in the central parts of the basin. The siltstones of the Patti Formation are commonly parallel stratified with occasional soft sedimentary structures e.g slumps, and other structures such as wave, ripples, convolute laminations, load structures. Trace fossils (especially *Thallasanoides*) are frequently preserved. Interbedded claystones are generally massive and kaolinitic, whereas the interbedded grey shales are frequently carbonaceous. The subsidiary sandstone units of the Patti Formation are more texturally and mineralogically mature compared with the Lokoja sandstones. The predominance of argillaceous rocks, especially siltstones, shales and claystones in the Patti Formation requires suspension and settling of finer sediments in a quiet low energy environment probably in a restricted body of water [33]. The abundance of woody and plant materials comprising mostly land-derived organic matter, suggests prevailing fresh water conditions. However, biostratigraphic and paleoecologic studies by Petters [34] have revealed the occurrence of aranaceous foraminfera in the shales of the Patti Formation with an assemblage of *Ammobaculites,Milliamina, Trochamina* and *Textularia* which are essentially cosmopolitan. Akande et al. [15], Ojo and Akande [35] studied the southeastern parts of the Bida Basin, parts of which are underlain by the Patti Formation and found an abundance of well-preserved pollens, spores and dynocysts in the shale and claystone section very well exposed at Ahoko village along the Lokoja-Abaji road. The pollen and spores are those from angiosperms, pteridophytes, gymnosperms and palmae. They are the basis for the assignation of the Maastrichtian age to the formation. Additionally, the presence of the dynocysts *Dinogymnium acuminatum, Senegalinium bicavatum* and *Paleocystodinium australinium* indicates marine depositinal setting for the lower parts of the formation in the early parts of Maastrichtian. The abundance of the pollen of the palms *Echitriporites* and *Longapertites* as well pteridophytes indicate the predominance of humid tropical paleoclimate.

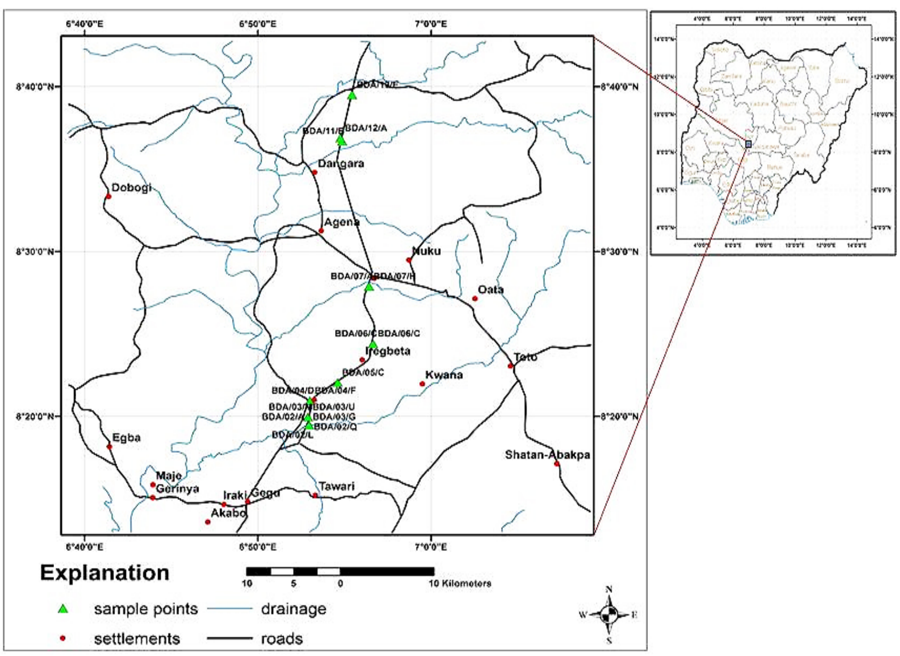

Figure 3. Location map of the study area

3. Materials and Methods of Study

A systematic geological mapping was carried out within the study area for lithologic characterization and more so to know if the rock units have potential for mineralization, using of GPS, measuring tapes, compass clinometers, hammer and digital camera was adopted. Lithologic units were described based on their physical attributes such as colour, grain size, geometry, bedding and sedimentary structure as they appear on the outcrop and core samples. The photographs of outcrop sections were taken and lithologic profiles of the outcrop locations were drawn to scale along Lokoja-Abaji-Abuja express way (Table 1 and Figure 4). Sixteen representative sandstone samples were selected for geochemical analysis. The initial preparation involving crushing and pulverizing were carried out at National Geosciences Research Laboratories, Kaduna. The samples were then analysed using an ICP-MS (Model: Perkin-Elmer Elan 6000) on a powdered 3-5 g sandstone samples at the Acme Lab. Ltd., Canada for major, trace and rare-earth elemental compositions. It was digested in a graphite crucible blended with 1.5 g Lithium metaborate/tetraborate ($LiBO_2$/$LiB4O_7$) flux by weighing 0.2 g aliquot. Placed in an oven, the crucibles were heated for 30 minutes at 980 °C. The cooled bead was dissolved in 5% HNO_3 (nitric acid grade ACS diluted in demineralized water). Sample sequences were supplemented with calibration norms and reagent blanks. The basic set of 34 components including Ba, Co, Cs, Ga, Hf, Nb, Rb, Sn, Sr, Ta, Th, U, V, Y, Zr, La, Ce Pr, Nd, Sm, Eu, Gd and Lu was established for the sandstone samples. Digested in Aqua Regia, a second 0.5 g sample was analysed by ICP-MS to determine Au, Ag, As, Bi, Cd, Cu, Hg, Mo, Ni, Pb, Sb, Se and Zn. The ICP-AES (Spectro Ciros Vision) was used to determine major oxides and certain trace elements, such as SiO_2, Al_2O_3, Fe_2O_3, CaO, MgO, TiO_2, P_2O_5, Cr_2O_5, Ba, Nb, Ni, Sr, Sc, Y and Zr. For both packages, loss on ignition (LOI) was determined by measuring the weight loss following 90 minutes of heating a 1.0 g split sample at 95 °C.

4. Results and Discussion

Field description

The lithologic sections of the Patti Formation reveal alternating sequences of shales, claystone, siltstone and sandstone with ferruginous mudstone interbeds as shown in Table 1 and Figure 4.

Table 1. Lithological profile of BDA/03

Sample No	Thickness (m)	Depth (m)	Description					
			Colour	*Grain*	*Sorting*	*Diagenesis*	*Geometry*	*Rk Type*
1	0.57	0-0.57	R-B	Fine		M-VI	WP	Sst
2	1.92	0.57-2.49	Grey			MI	PP	Cst
3	0.23	2.49-2.72	R-G	Fine	Well	M-VI	WP	Sst
4	0.61	2.72-3.33	Grey			MI	PP	Cst
5	0.32	3.33-3.65	R-G	Fine	Well	MI	WP	Sst
6	0.65	3.65-4.3	Grey			MI	PP	Cst
7	0.35	4.3-4.65	R-B	Fine	Well	M-VI	WP	Sst
8	0.83	4.65-5.48	Grey			MI	PP	Cst
9	0.41	5.48-5.89	R-B	Fine	Well	M-VI	WP	Sst
10	3.29	5.89-9.18	Grey			VI	PP	Cst
11	0.45	9.18-9.63	R-G	Fine	Well	VI	WP	Sst
12	0.33	9.63-9.96	Grey			MI	PP	Cst
13	0.20	9.96-10.16	R-G	Fine	Well	VI	WP	Sst
14	1.29	10.16-11.45	Y-G			M-VI	PC	Cst
15	0.48	11.45-11.93	R-G	Fine	Well	MI	WP	Sst
16	0.44	11.93-12.37	LG			MI	PP	S/st
17	0.81	12.37-13.18	Grey			MI	PC	Cst
18	0.21	13.18-13.39	Grey			MI	PP	Cst
19	0.46	13.39-13.85	Grey			MI	PP	Sh
20	0.33	13.85-14.18	R-G			MI	PP	Cst
21	1.12	14.18-15.3	Grey			MI	PP	Sh
22	0.65	15.3-15.95	Grey			MI	PP	Cst

B= Black M=Moderate WP=wavy planar Sst= Sandstone R=Red V=Very PP= Planar parallel
Cst=Claystone G=Grey I=Indurated PC=Planar cross S/st=Siltstone Y=Yellow Sh=Shale

The sandstone units encountered are characterised with fine grained variety, although, medium and coarse grained sandstones cannot be written off. These units consist of wedged beds between 0.17 m and to relatively over 6 m thick, exhibiting variety of colours ranging from dirty white through grey to yellowish and reddish brown. Observed sedimentary structures are cross laminations (Figure 5a), flaser bedding (Figure 5b), Strike and dip measurement (Figure 5c), liesegang rings and burrows (vertical and inclined) (Figure 5d) but most of the sandstone units are conspicuously indurated forming series of interconnected concretions giving the bed a wavy or rippled geometry (Figure 5e).

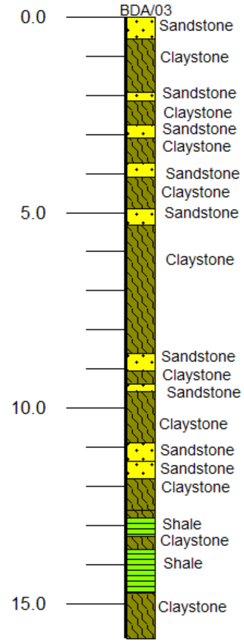

Figure 4. 2D strip log of BDA/03 location

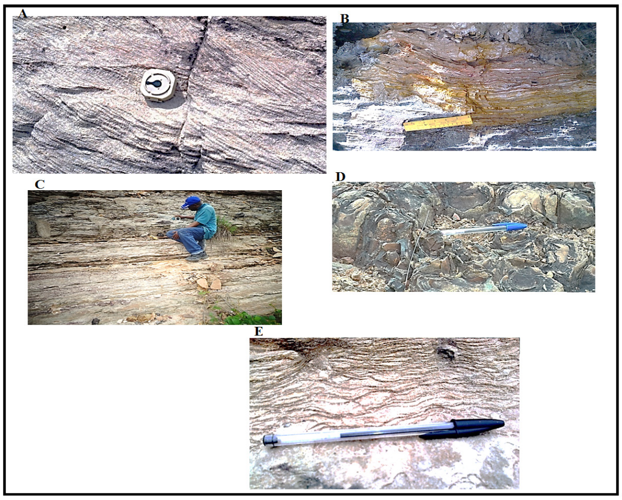

Figure 5. a) Cross lamination in medium grained sandstone near Abaji, along the Lokoja- Abaji –Abuja highway, **b)** Sandstone with flaser bedding exposed at Ahoko, along Lokoja - Abuja highway, **c)** Geologist taking strike and dip of siltstone near Ahoko, along Lokoja Abaji-Abuja highway, **d)** Liesegang rings in sandstone concretion at Ahoko, along the Lokoja-Abaji –Abuja highway, **e)** Wavy lamination in sandstones exposed along the Lokoja Abaji-Abuja highway.

4.1 Whole Rock Geochemistry

The whole rock geochemical concentrations of major, trace, rare earth elements, and values of other geochemical parameters obtained from the investigated sandstones are documented in Tables 2, 3, and 4. This concentration is proposed to be dependent largely on the composition of the precursor/source rocks and suites of sedimentary processes (weathering and diagenetic) [36,37].

Major oxides

The major elemental concentration is presented in Table 2. Observed result revealed that SiO_2 and Al_2O_3 have the dominant element concentration (Table 2). The SiO_2 concentrations range from 73.9% to 86.2%, Al_2O_3 ranges between 6.7% and 17.1%, Fe_2O_3 concentrations range from 1.1% to 1.9%, K_2O concentrations range from 0.1% to 0.7% and MgO ranges from 0.01% to 0.03%. However, the following are low in concentration; CaO (0.02%~0.04%), Na_2O (0.00%~0.01%), P_2O_5 (0.02%~0.04%), MnO (0.00%~0.01%) and TiO_2 (0.31%~0.84%) which led to the removal of ferromagnesian minerals and feldspars as a result of weathering. Low TiO_2 implies low presence of Ti-opaque minerals and rutile in the sandstone while lack of MnO is most likely due to dissimulator of manganese diminution by the action of microbes or source-area composition (Table 2). The recorded low K_2O content suggest low amount of illite or feldspar present [38]. The MgO content is relatively low indicating non-association with dolomitisation and most samples have low P_2O_5 content; depletion implying low amount of accessory phases, such as apatite and monazite. The ratio of SiO_2/Al_2O_3 for the Patti sandstone indicates high silica to alumina composition, while the low ratio of K_2O/Al_2O_3 reveal low K-bearing mineral contents associated with alumina. Obtained Al_2O_3/TiO_2 ratios denote abundance of alumina relative to titanium oxide [39] (Table 2).

Trace and rare earth element geochemistry

The value for the distribution of trace element for the Patti sandstone is listed in Table 3. The sandstone revealed high variation in concentration of trace elements, this attribute usually point towards a shared provenance, weathering, and tectonic setting [20,40,41]. Patti sandstones are enriched in Ba (Av. 622.94), Sr (Av. 153.63), Rb (Av. 55.08) and Zr (Av. 51.86) all in ppm. Ba content account for the highest in concentration for almost the studied sandstone samples. The Patti sandstone showed relative similar composition when compared with UCC (Figure 6).

Obtained high variation in geochemical ratios of Zr/Sc (0.86 ppm ~ 39.19 ppm) and Zr/Hf (27.77 ppm ~ 103.19 ppm) for the Patti sandstone suggest occurrence of zircon enrichment [41,21] (Table 3). According to Bhatia and Crook [40], Dabard [42], La/Sc ratio can be used for rock maturity determination, commonly within the range from 3 to 9. The sandstones under investigation, show large variation in La/Sc ratio, which ranges from 1.27 to 10.91 (Table 3) suggesting the matured nature of the Patti sandstone.

The investigated Patti sandstone revealed: ∑REE (82.73 ppm ~ 327.50 ppm; Av. ~ 209.14 ppm), higher light rare earth elements (LREE) (8.60 ppm ~ 320.20 ppm; Av. ~ 192.29 ppm) than heavy rare earth elements (HREE) (2.50 ppm ~ 20.66 ppm; Av. 9.76), high LREE/H- REE ratios (1.51 ~ 87.69; Av. 29.01) and negative Eu/Eu* (0.33 ~ 0.88; Av. 0.67) with chondrite-normalized patterns characterised by light REE (LREE) enrichment, flat heavy REE (HREE) patterns, and negative Eu anomalies [43] (Table 4; Figure 7) indicative of passive margin tectonic setting.

Table 2. Major elements concentration (in wt%) of sandstone samples collected from Patti Formation.

Major oxides	SiO_2	FeO_3	CaO	MgO	Al_2O_3	Na_2O	K_2O	MnO	T_iO_2	P_2O_5	Cr_2O_3	Al_2O_3/TiO_2	K_2O/Al_2O_3	SiO_2/Al_2O_3	DF1	DF2
BDA /02/A	74.09	1.09	0.03	0.01	16.35	0.01	0.07	0.01	0.41	0.04	0.01	39.88	0.004	4.53	–3.47	–2.19
BDA /02/L	74.07	1.07	0.03	0.01	16.4	0.01	0.07	0.01	0.39	0.03	0.01	42.05	0.004	4.52	–3.36	–2.16
BDA/02/Q	74.01	1.06	0.03	0.01	16.5	0.01	0.06	0.01	0.42	0.04	0.01	39.20	0.004	4.49	–3.44	–1.94
BDA /03/G	74.9	1.1	0.35	0.01	17	0.01	0.05	0.01	0.32	0.04	0.01	53.13	0.003	4.41	–3.07	–2.25
BDA/03/M	73.9	1.12	0.34	0.01	16.9	0.01	0.02	0.01	0.31	0.04	0.01	54.52	0.043	4.37	–7.13	–2.07
BDA/03/U	74	1.09	0.32	0.01	17.1	0.01	0.03	0.01	0.32	0.04	0.01	53.44	0.043	4.33	–6.27	–1.36
BDA /04/D	75.1	1.1	0.04	0.01	16.2	0.01	0.08	0.01	0.31	0.04	0.01	52.26	0.005	4.65	–3.38	–2.19
BDA /04/F	75	1.1	0.03	0.01	16.1	0.01	0.07	0.01	0.32	0.03	0.01	50.31	0.004	4.6	–3.35	–1.85
BDA /05/C	74.9	1.2	0.04	0.01	16.2	0.01	0.09	0.01	0.3	0.04	0.01	54.00	0.006	4.62	–3.52	–2.33
BDA /06/C	75	1.2	0.04	0.01	16.3	0.01	0.08	0.01	0.3	0.04	0.01	54.33	0.005	4.60	–3.53	–2.13
BDA /06/D	75.1	1.1	0.03	0.01	16.1	0.01	0.09	0.01	0.4	0.04	0.01	40.25	0.006	4.66	–7.41	–2.57
BDA /07/A	75.13	1.27	0.02	0.01	16.25	0.01	0.08	0.01	0.31	0.04	0.01	52.42	0.005	4.62	–3.72	–1.57
BDA /07/H	86.24	1.92	0.02	0.03	6.79	0.01	0.08	0.01	0.84	0.02	0.01	8.08	0.012	12.70	–2.60	–2.89
BDA /11/B	75.2	1.8	0.02	0.03	16.3	0.01	0.08	0.01	0.8	0.03	0.01	20.38	0.005	4.63	–3.00	–7.86
BDA /12/A	75	1.6	0.02	0.02	16.4	0.01	0.08	0.01	0.82	0.04	0.01	20.00	0.005	4.57	–2.85	–2.37
BDA /13/E	74.9	1.5	0.02	0.01	16.25	0.01	0.07	0.01	0.79	0.03	0.01	20.57	0.004	4.61	–4.20	–8.09

Table 3. Trace element concentration (ppm) in sandstone samples of Patti Formation

Sample	Ni	Zr	Hf	Be	Th	U	Ba	La	Co	Zr	As	Cd	Sb	Sc	Sn	Rb	Sr	Ta	Nb	Zr/Sc	Zr/Hf	La/Sc
BDA/02/A	10.0	48.5	0.47	4	5.4	2.8	275	17.5	10.6	48.5	2.2	0.11	0.08	2.7	1.4	9.2	135	0.8	10.15	17.96	103.19	6.48
BDA/02/L	2.8	36.9	1.13	1	12	3	87	88.3	0.7	36.9	2.1	0.12	0.11	8.2	1.6	4.2	63	0.4	5.55	4.50	32.65	10.77
BDA/02/Q	2.7	37.0	1.13	2	13	3.2	89	88.4	0.9	37.0	2.0	0.11	0.12	8.1	1.7	4.3	60	0.5	5.65	4.57	32.74	10.91
BDA/03/G	2.9	37.6	1.12	1	14	2.9	85	87.9	0.8	37.6	2.2	0.12	0.10	8.4	1.7	4.4	66	0.5	5.5	4.48	33.57	10.46
BDA/03/M	2.9	37.7	1.14	1	11.2	2.8	87	89	0.8	37.7	2.2	0.11	0.10	8.4	1.7	4.4	63	0.5	5.67	4.49	33.07	10.59
BDA/03/U	4.7	64.3	2.27	1	14.4	4.7	90	27.6	2.0	64.3	11.4	0.11	0.16	6.8	1.7	3.2	15	2.2	16.21	9.46	28.33	4.06
BDA/04/D	67.0	87.4	2.63	2	14.8	3.2	875	45.1	23.2	87.4	7.2	0.26	0.12	19.1	10.0	107.2	223	1.1	16.85	4.58	33.23	2.36
BDA/04/F	75.2	105.5	2.96	4	10.9	2.1	909	29.5	29.3	105.5	6.6	0.35	0.10	23.3	4.2	106.5	167	1.3	18.21	4.53	35.64	1.27
BDA/05/C	40.3	72.0	2.5	2	16.2	5.4	804	37.4	27.0	72.0	0.5	0.10	0.09	16.0	2.9	104.3	363	1.8	17.23	4.50	28.80	2.34
BDA/06/C	49.7	25.8	0.82	3	7.5	2.1	1751	31.5	16.5	25.8	0.8	0.05	0.16	12.4	2.2	60.7	114	1.0	7.09	2.08	31.22	2.54
BDA/6/D	7.5	141.1	4.5	<1	19.6	3.7	88	31.6	2.5	141.1	2.2	0.21	0.16	3.6	2.9	6.7	20	2.5	31.01	39.19	31.36	8.78
BDA/07/A	49.6	25.7	0.79	3	8	2.2	1698	37.5	16.2	25.7	0.6	0.06	0.17	12.5	2.1	60.6	124	1.0	7.05	2.06	32.53	3
BDA/07/H	40.2	72.2	2.6	2	15.5	5.5	750	31.7	27.0	72.2	0.6	0.10	0.08	16.1	2.8	104.4	350	1.9	18.10	4.48	27.77	1.97
BDA/11/B	49.7	25.8	0.81	3	7.8	2.5	1740	52.9	16.5	25.8	0.8	0.05	0.16	12.4	2.2	60.7	116	1.0	7.09	2.08	31.85	4.27
BDA/12/A	8.4	3.2	0.07	<1	4.2	0.3	186	13.6	9.7	3.2	1.7	0.06	0.05	3.7	2.1	35.7	489	0.4	6.58	0.86	45.71	3.68
BBB/13/E	20.2	9.1	0.26	<1	17.4	1.4	453	53.4	7.1	9.1	6.7	<0.02	0.09	5.2	4.4	204.9	90	0.3	5.37	1.75	35	10.27

Table 4. Rare earth element concentration (ppm) of sandstone samples from Patti Formation.

	Light Rare Earth Elements (LREE)						Rare Earth Elements (HREE)								Ratios				
Sample	La	Ce	Pr	Nd	Sm	Eu	Gd	Tb	Dy	Ho	Er	Tm	Yb	Lu	∑REE	LREE	HREE	LREE/ HREE	(Eu/Eu*
BDA/02/A	17.5	37.73	3.6	14.4	2.7	0.6	1.8	0.2	1.8	0.3	0.8	0.1	1	0.2	82.73	78.33	4.4	17.8	0.84
BDA/02/L	88.3	142.6	16.2	55.4	6.8	1.3	5.2	0.6	3.2	0.3	1.4	0.2	1.6	0.2	323.3	315.8	7.5	42.11	0.67
BDA/02/Q	88.4	146.2	16.8	55.5	6.7	1.3	5.3	0.6	3	0.3	1.4	0.2	1.6	0.2	327.5	320.2	7.3	43.86	0.67
BDA/03/G	87.9	145.2	17.1	54.9	7	1.25	5.3	0.7	3.1	0.3	1.4	0.2	1.6	0.2	326.15	318.65	7.5	42.89	0.63
BDA/03/M	89	137.96	15.9	53.3	9.6	2	7.9	1.2	5.2	0.8	2	0.3	1.5	0.2	326.86	315.66	11.2	28.18	0.71
BDA/03/U	27.6	58.52	7.4	26.3	5.1	0.9	4.9	0.5	3.2	0.6	1.6	0.2	1.7	0.2	138.72	130.72	8	16.34	0.33
BDA/04/D	45.1	102.12	12.1	46.2	9.3	2.2	8	0.9	4.8	0.6	1	0.2	1.4	0.2	234.12	225.02	9.1	24.73	0.78
BDA/04/F	29.5	68.19	8	33	6.9	1.6	6.3	0.8	3	0.4	0.6	0.1	1	0.2	159.59	153.49	6.1	25.16	0.75
BDA/05/C	37.4	80.79	8.8	33.4	6.7	1.2	5.1	0.6	3.1	0.4	1.3	0.2	1.6	0.2	180.79	173.39	7.4	23.43	0.63
BDA/06/C	31.5	75.03	8.3	32.2	5.7	1.7	6.4	1.1	7.6	0.5	5	0.8	4.8	0.8	181.43	160.83	20.6	7.81	0.84
BDA/6/D	31.6	74	8.5	33.2	5.8	1.7	6.5	1.2	7.5	0.5	5	0.8	4.8	0.8	181.9	161.3	20.6	7.83	0.85
BDA/07/A	37.5	80.6	8.9	33.5	6.8	1.3	5.6	0.5	3.5	0.4	1.3	0.2	1.6	0.2	181.9	174.2	7.7	22.63	0.67
BDA/07/H	31.7	75.1	8.4	33.1	5.8	1.8	6.5	1.1	7.5	0.5	5.2	0.8	4.6	0.8	182.9	162.4	20.5	7.92	0.7
BDA/11/B	52.9	103.14	10.6	35.8	6.1	0.8	5.2	0.6	2.9	0.4	1	0.2	1.2	0.2	221.04	214.54	6.5	33.01	0.88
BDA/12/A	13.6	32.6	3.9	19.2	4.3	0.6	3.7	0.4	2.7	0.4	1.1	0.2	0.8	0.1	83.6	8.6	5.7	1.51	0.52
BBB/13/E	53.4	99.03	12.4	42	6.7	1.2	4.5	0.4	1.6	0.1	0.2	0.1	0.2	<0.1	221.73	219.23	2.5	87.69	0.37

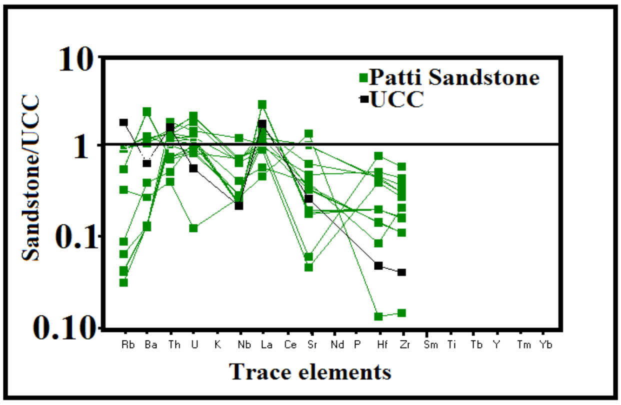

Figure 6. Trace element normalized diagram for the Patti sandstone samples, normalized against the average upper continental crust [43]. A horizontal line for sandstone/upper continental crust value of 1 is included for reference.

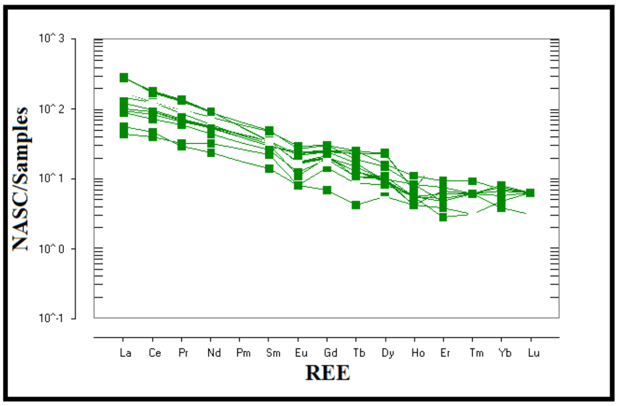

Figure 7. NASC-Chondrite normalised rare elements plot of the investigated Patti sandstone (After Boynton [44]).

4.2 Classification of the Patti Sandstone

For the classification of Patti sandstone, the classification diagrams of Heron [45] and Petijohn et al. [46] were employed. The classification diagram revealed that the Patti sandstone varied mainly within the region of lith-arenites, subarkose, and Fe-sands (Figure 8). The observed variation, according to Lindsey et al. [47] can be attributed to a wide range in the differences of proportion with relation to possible matrix, feldspar, and lithic components and possibly as a result of sedimentary processes [20].

4.3 Source Area Weathering

In the determination and evaluation of chemical weathering intensity, many authors, although not limited to Nesbitt and Young [48]; McLennan et al. [21]; Li and Yang [49]; Roy and Roser [50]; Yang et al. [51]; Dinis et al. [52]; Bal-Akkoca et al. [53]; Overare and Osokpor [54]; Bolarinwa et al. [55] have discovered chemical index of alteration (CIA) as a potent tool for the degree of chemical weathering determination. For the sandstone from Patti Formation under investigation as documented in Table 5 revealed a CIA range from 98.1% to 99.8%, this suggests intense weathering in the source area. CIA estimate includes the use of K_2O, a mobile oxide; in sediments where potassium has been leached, its applicability maybe restricted (Condie et al. [56]). The CIA was followed by the chemical index of weathering (CIW) with values ranging from 98.11 to 99.97 (Table 5), reflects an intense degree of weathering in the source area. Also used was the plagioclase index of weathering (PIA), PIA aids and measures trend in weathering of feldspars to clay minerals [22]. The high PIA values (97.89 ~ 99.82; Table 5) obtained for the Patti sandstones, suggests that almost all of the plagioclase present have been altered into clay minerals [54,55].

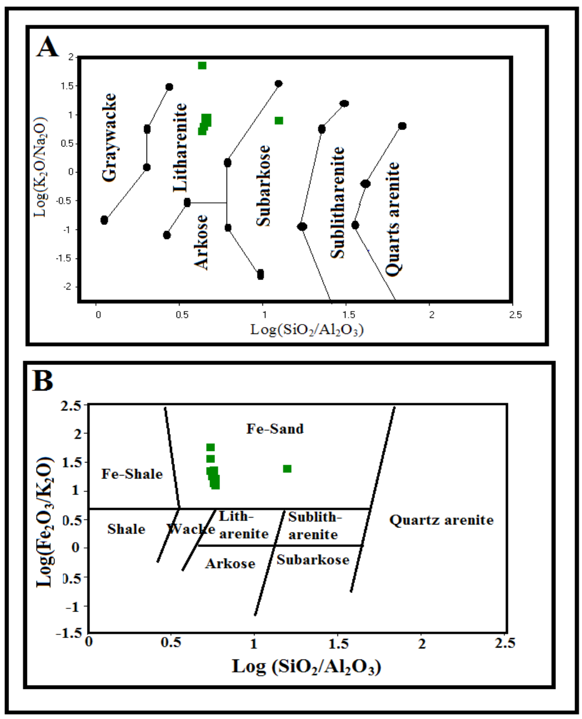

Figure 8. Bivariate chemical classification plot of the investigated sandstones of Patti Formation based on **A)** log (SiO_2/Al_2O_3) vs. log (Na_2O/K_2O) (After Herron [45]) and **B)** Log (SiO_2/Al_2O_3) vs. log (Na_2O/K_2O) diagram for the sands (Pettijohn et al. [46]).

Table 5. Calculated geochemical ratios for the investigated Patti sandstone.

Ratios → Sample No:↓	CIA	MIA	CIW	ICV	PIA	WIP	αNa	αCa	αMg	αK	αBa	αRb	αSr	Al/Mg	K/Na	Th/U	Th/K	Rb/K	Sm/Na
BDA /02/A	99.3	98.6	99.76	0.096	99.75	27.00	331.23	132.56	304.23	44.19	2.84	0.02	2.27	1,442.06	7.85	1.93	0.07	0.02	0.04
BDA /02/L	99.3	98.6	99.76	0.095	99.76	27.00	332.24	132.97	305.17	44.33	9.02	0.04	4.89	1446.48	7.85	4.00	0.16	0.007	0.09
BDA/02/Q	99.4	98.8	99.76	0.094	99.76	35.00	334.27	133.78	307.03	52.03	8.87	0.04	5.16	1455.3	6.73	4.06	0.18	0.009	0.08
BDA /03/G	93.8	87.6	97.93	0.128	98.00	77.00	344.40	11.79	316.33	64.33	10.52	0.04	4.84	1499.4	5.61	4.83	0.19	0.01	0.09
BDA/03/M	94.	88	97.97	0.133	97.89	58.00	342.37	12.07	398.55	4.44	10.22	0.04	5.04	1490.58	80.77	4.00	0.15	0.0007	0.13
BDA/03/U	94.4	88.8	98.11	0.126	98.02	56.00	346.42	12.97	318.19	4.43	9.09	0.06	21.40	1508.22	81.89	3.06	0.19	0.0005	0.07
BDA /04/D	99.3	98.6	99.69	0.093	99.69	29.00	328.19	98.28	301.44	38.31	0.89	0.002	1.37	1428.83	8.97	4.63	0.20	0.16	0.13
BDA /04/F	99.3	98.6	99.69	0.093	99.75	31.00	326.17	130.54	299.58	43.51	0.85	0.002	1.81	1420.02	7.85	5.19	0.15	0.18	0.09
BDA /05/C	99.1	81.2	99.69	0.099	99.69	49.00	328.19	98.28	301.44	34.06	0.94	0.002	0.84	1428.83	10.09	3.00	0.22	0.14	0.09
BDA /06/C	99.2	98.4	99.69	0.098	99.69	45.00	330.22	98.89	384.40	38.55	0.45	0.003	2.68	1437.67	8.97	3.57	0.10	0.09	0.08
BDA /06/D	99.2	98.4	99.75	0.10	99.75	47.00	326.17	97.67	299.58	38.08	8.75	0.03	15.11	1420.02	8.97	5.30	0.26	0.01	0.08
BDA /07/A	98.1	96.2	98.82	0.104	99.81	42.00	329.21	131.75	302.37	38.43	0.46	0.003	2.46	1433.25	8.97	3.64	0.11	0.09	0.09
BDA /07/H	98.4	98.8	99.56	0.424	99.55	45.00	340.15	203.72	103.57	39.71	1.07	0.002	0.90	90.90	8.97	2.82	0.21	0.16	0.08
BDA /11/B	99.3	99.6	99.82	0.099	99.82	44.00	330.22	197.98	100.54	38.55	0.45	0.003	2.64	476.57	8.97	3.12	0.11	0.09	0.08
BDA /12/A	99.3	98.6	99.82	0.106	99.82	43.00	332.24	198.99	151.32	38.79	4.22	0.005	0.63	717.26	8.97	14	0.06	0.05	0.06
BDA /13/E	99.4	98.8	99.82	0.098	99.39	38.00	329.21	197.17	302.37	43.92	1.72	0.0008	3.89	1433.25	7.85	12.42	0.24	0.35	0.09

The CIA= Chemical index of Alteration ($100[Al_2O_3/(Al_2O_3+CaO+Na_2O+K_2O)]$)
The PIA= Plagioclase Index of Alteration ($100[(Al_2O_3-K_2O)/(Al_2O_3+CaO+Na_2O-K_2O]$)
The CIW= Chemical Index of Weathering ($100[Al_2O_3/(Al_2O_3+CaO+Na_2O)]$)
The MIA = Mineralogical index of alteration (2*(CIA-50))
The ICV = ($Fe_2O_3+K_2O+Na_2O+MgO+MnO+TiO_2/Al_2O_3$).
The WIP = Weathering Index of Parker ($100[(2Na_2O/0.35)+(MgO/0.9)+(2K_2O/0.5)+(CaO/0.7)]$)
α = (Al/E) sample/ (Al/E) UCC, where E = mobile elements (Na, Ca, Sr, Mg, K and Ba).

Similarly, obtained values for the Mineral Index of Alteration (MIA) (88.00 ~ 99.60; Table 5) and WIP (27.00 ~ 77.00; Table 5) also revealed intense weathering in the source area, and they are unswerving with obtained record from the CIA, CIW, and PIA computation. Thus, the indices used are complementary as they show similar trends.

To further determine the degree of weathering in the source area, a more consistent and reliable indices put forward by Garzanti et al. [57] was also employed, this made use of ratio for a single mobile element (e.g. Mg, Ca, Na, Sr, K, Ba) to a non-mobile element with similar magmatic compatibility (most appropriate-Al), called α value. The $\alpha^{Al}{}_{E}$ values for any element (E) are defined as $\alpha^{Al}{}_{E}$ = Al/E $_{sample}$ / Al/E $_{UCC}$ Garzanti et al. [57]. Obtained values of $\alpha^{Al}{}_{E}$ for the investigated sandstone samples in Table 6 revealed that Sodium (326.17 $\alpha^{Al}{}_{Na}$ < 344.40) is more mobile than magnesium (100.54 $\alpha^{Al}{}_{mg}$<398.55), calcium (12.07 $\alpha^{Al}{}_{Ca}$<198.99), pottassium (4.43 $\alpha^{Al}{}_{K}$< 64.33), strontium (0.84 $\alpha^{Al}{}_{E}$ 21.40), barium (0.45 $\alpha^{Al}{}_{Ba}$ <10.52) and rubidium (0.0008 $\alpha^{Al}{}_{Rb}$<0.06). The obtained high variation in value determined for Mg, Ca, Na, K, Ba, Rb and Sr can be interpreted as a sign of strong weathering control [30,55]. This was supported with a calculated weathering parameters: Th/U and Rb/K [58,55] (Table 5).

Also used in evaluating the degree of weathering for the Patti sandstone is the Al_2O_3-(CaO^*+Na_2O)-K_2O ternary plot of Nesbit and Young [48], this model monitors the progress of weathering by illustrating the link between Al_2O_3 (aluminous clays), CaO+Na_2O (Plagioclase) and K_2O (K- feldspar) [59]. All the sediments plot at the Al_2O_3 peak suggesting an intense chemical weathering (Figure 9a). This was supported by the CIA vs. SiO_2 plot of Nesbitt and Young [48] (Figure 9b), which also gave an interpretation in a similar way to the A-CN-K diagram, with the field of kaolinite representing intense weathering and significant removal of the alkali and alkali earth elements.

4.4 Paleo-climatic Conditions

Studies on paleoclimatic conditions have proven to be a potent tool in the understanding of processes involved during weathering of a source area. According to Suttner and Dutta [61] and supported by Overare and Osokpor [54]; Bolarinwa et al. [55] stated that major elemental compositions offer useful indications in relation to the climatic conditions that occurred during the deposition of sedimentary rocks as climate, in general, affects the modification of minerals, transport, and source rock chemistry. In view of the fact that the degree of weathering is primarily a function of climate and tectonic setting, the CIA provides a clue on the source rock weathering and paleoclimatic condition [62], whereby increased degree of weathering might imply a lessen activity of tectonism and/or a variation in climate from arid toward warm and humid conditions [48]. Thus, according to Fedo et al. [60], Tang et al. [63], Overare and Osokpor [54] stated that CIA values of ≤50, suggests cool and/or arid climatic conditions devoid of profuse rainfall, while values >80 are linked to humid climates resulting in a high-degree alteration of source rocks [64]. The obtained high CIA values for the Patti sandstones under investigation is consistent with values >80 implying a steady-state of weathering, possibly under a warm/humid climate. This was confirmed by the bivariate plot of Sutner and Dutta [61] to evaluate the maturity of the sandstone as a function of climate. On this diagram, the Patti sandstones plot basically in the region of humid climate (Figure 10).

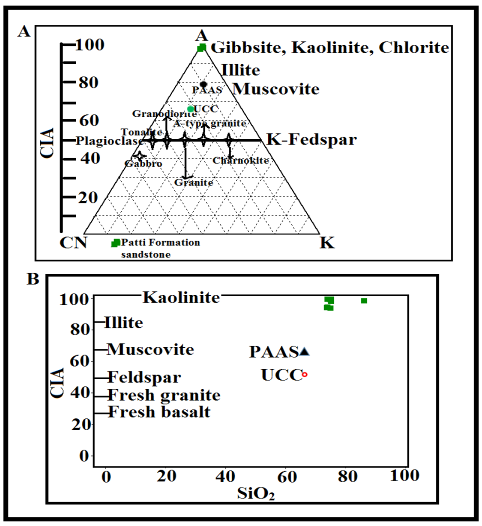

Figure 9. Plot of **A**): Al_2O_3-(CaO^*+ Na_2O)-K_2O for the sediments (Nesbith and Young [48]; Fedo et al. [60]) and **B**): CIA versus SiO_2 (Nesbitt and Young [48]). B). Note that the sediments are clustering around a point.

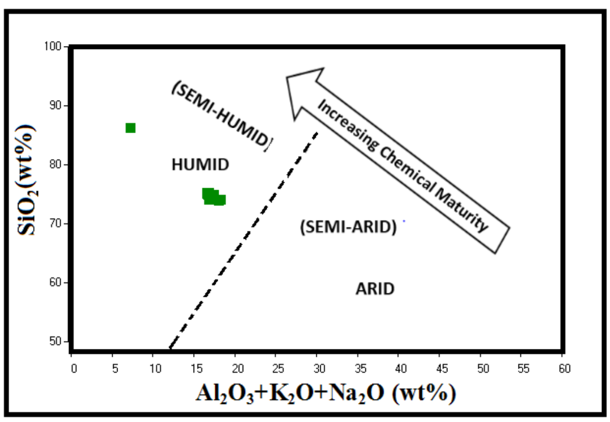

Figure 10. Bivariate plot of SiO_2 vs. Al_2O_3+ K_2O + Na_2O for Patti sandstone indicating chemical maturity as a function of climate (after Suttner and Dutta [61]).

4.5 Paleo-tectonic Setting

Geochemical records and parameters associated with siliciclastic sediments are common potential tools to establish the tectonic setting of known sedimentary basins [65,66,39,17]. McLennan et al. [65] and Ojo et al. [17], documented that chemical compositions, sandstones can be categorized into different tectonic settings; magmatic island arcs (average SiO_2: <58%, K_2O/Na_2O < 1), Andean-type continental margins (SiO_2: 68% to 74%, K_2O/Na_2O < 1), Atlantic-type continental margins (average SiO_2: <89%, K_2O/Na_2O > 1). Applying this parameter, the investigated Patti sandstone which ranged in SiO_2 from 74.01 wt% to 86.24 wt% (Table 3) and K_2O/Na_2O from 5 to 9 (Table 6), suggest an Atlantic-type continental margins that compares favourably in term of compositional characteristics with continental platform sands. Also employed in this investigation is the idea proposed by Bhatia [20] which puts forwards that sedimentary basins adjacent to oceanic island arcs will naturally demonstrate high ratios/values of Fe_2O_3/MgO (8%–14%), Al_2O_3/SiO_2 (0.24–0.33), TiO_2 (0.8%–1.4%) and lower K_2O/Na_2O (0.2–0.4) ratios while sandstones of basins adjacent to continental island arcs from oceanic island-arc types have lower Fe_2O_3/MgO (5%–8%), TiO_2 (0.5–0.75) and Al_2O_3/SiO_2 (0.15–0.22) and higher K_2O/Na_2O (0.4–0.8) ratios. It was stated further that sandstones from basins on active continental margins have very low Fe_2O_3/MgO (2%–5%), TiO_2 (0.25%–0.45%) and K_2O/Na_2O ratio ~1 while the passive margin sandstones are generally enriched in SiO_2 and depleted in Al_2O_3, TiO_2, Na_2O, CaO with K_2O/Na_2O ratio >1. The investigated Patti sandstones fall into the tectonic category of passive margin, because they contain high average SiO_2 (75.41 wt%) with K_2O/Na_2O ratio >1 (15.63) but relatively depleted in Fe_2O_3 (1.27 wt%), Al_2O_3 (15.82 wt%) and TiO_2 (0.46) (Tables 2 and 6).

Table 6. Ratios of some major elements of sandstone samples from Patti formation

Major oxides	**BDA /02/A**	**BDA /02/L**	**BDA/ 02/Q**	**BDA /03/G**	**BDA/ 03/M**	**BDA/ 03/U**	**BDA /04/D**	**BDA /04/F**	**BDA /05/C**	**BDA /06/C**	**BDA /06/D**	**BDA /07/A**	**BDA /07/H**	**BDA /11/B**	**BDA /12/A**	**BDA /13/E**
K_2O/Na_2O	7.00	7.00	6.00	5.00	72.00	73.00	8.00	7.00	9.00	8.00	9.00	8.00	8.00	8.00	8.00	7.00
Na_2O+K_2O	0.08	.08	0.07	0.06	0.83	0.74	0.09	0.08	0.10	0.09	0.10	0.09	0.09	0.09	0.09	0.08
$CaO+Na_2O$	0.04	0.04	0.04	0.36	0.35	0.33	0.05	0.04	0.05	0.05	0.04	0.03	0.03	0.03	0.03	0.03
$SiO_2+Al_2O_3$	90.44	90.47	90.51	91.90	90.80	91.10	91.20	91.10	91.20	91.30	91.20	91.38	93.03	91.50	91.40	91.15
Al_2O_3/SiO_2	0.22	0.22	0.22	0.23	0.23	0.23	0.21	0.21	0.22	0.22	0.21	0.22	0.08	0.22	0.22	0.22
Na_2O/K_2O	0.14	0.14	0.17	0.20	0.01	0.03	0.13	0.14	0.11	0.13	0.11	0.13	0.13	0.13	0.13	0.14
Al_2O_3/TiO_2	39.88	42.05	39.20	53.13	54.52	53.44	52.26	50.31	54.00	54.33	40.25	52.42	8.08	20.38	20.00	20.57
Fe_2O_3/Al_2O_3	0.07	0.07	0.06	0.06	0.07	0.06	0.07	0.07	0.07	0.07	0.07	0.08	0.28	0.11	0.10	0.10
Fe_2O_3/MgO	109	107	106	110	112	109	110	110	120	120	110		127	180	160	150
$Al_2O_3+K_2O+Na_2O$	16.43	16.48	16.57	17.06	17.63	17.84	16.29	16.18	16.30	16.39	16.20	16.34	6.88	16.39	16.49	16.33
$Al_2O_3/CaO+Na_2O$	408.75	410	412.5	47.22	48.29	51.82	324	402.5	324	326	402.5	541.67	226.33	543.33	546.67	541.67
K_2O/Al_2O_3	0.004	0.004	0.004	0.003	0.043	0.043	0.005	0.004	0.006	0.005	0.006	0.005	0.012	0.005	0.005	0.004
$Fe_2O_3/MgO/Na_2O+K_2O$	13.75	13.5	15.29	18.5	1.55	1.49	12.33	13.88	12.10	13.44	11.10	14.22	21.67	20.33	18.00	18.88
$Log(SiO_2/Al_2O_3)$	0.67	0.66	0.65	0.64	0.64	0.64	0.67	0.67	0.66	0.66	0.67	0.67	1.10	0.66	0.66	0.66
$Log(Fe_2O_3/K_2O)$	1.19	1.18	1.25	1.34	1.56	1.49	1.14	1.20	15.00	1.18	1.08	1.20	1.38	1.35	1.30	1.33
$Log(K_2O/Na_2O)$	0.85	0.85	0.78	0.70	1.86	1.86	0.90	0.85	0.95	0.90	0.95	0.90	0.90	0.90	0.90	0.85
$Log(Na_2O/K_2O)$	–1.10	–1.10	–1.15	–1.22	–0.08	–0.13	–1.05	–1.10	–1.00	–1.05	–1.00	–1.05	–1.05	–1.05	–1.05	–1.10
$Log(Fe_2O_3+MgO/Na_2O+K_2O)$	1.14	1.13	1.18	1.27	1.55	0.19	1.09	1.08	1.08	1.13	1.05	1.55	1.34	1.31	1.26	1.28

Presence of REEs in sandstones also give clues to tectonic setting of a basin. McLennan et al. [65] and McLennan and Taylor [67] proposed that continental margin sediments are generally enriched with ΣREE, LREE and negative Eu/Eu*, while sediments from oceanic arcs are low in ΣREE and LREE but lack negative Eu/Eu*. In this study, obtained average values of ΣREE (209.64 ppm), ΣLREE (195.78), LREE/HREE (27.78) and negative Eu/Eu* (0.68) (Table 4) for the Patti sandstones suggest is consistent with a passive margin tectonic setting.

Also used for the tectonic setting appraisal are discrimination diagrams based on the bivariate plots of log (K_2O/Na_2O) vs. SiO_2 and SiO_2/Al_2O_3 vs. K_2O/Na_2O as proposed by Roser and Korsch [27], which are very helpful in the discrimination of basins into Oceanic island-arc, Continental island-arc, Active continental margin and Passive margin where increasing values of K_2O/Na_2O and SiO_2 implies a modification from ARC → ACM → PM. Obtained high values of K_2O/Na_2O and SiO_2 as plotted in Figure 11 suggest a comparatively stable or passive margin tectonic environment of deposition for the Patti sandstones.

In recent research into tectonic environments of deposition for sediments, many authors although not limited to LaMaskin et al. [68]; Verma and Armstrong-Altrin [69]; Armstrong-Altrin, et al. [70], Zaid [39] cautioned the poor presentation of the major element conventional discrimination diagrams proposed by Bhatia [20] and Roser and Korsch [40] to deduce accurate tectonic environment of unknown basins. Verma and Armstrong-Altrin [69] suggested two discrimination function diagrams for tectonic discrimination of siliciclastic sediments: one for high-silica rocks [(SiO_2)adj = 63% to 95%] and one for low-silica [(SiO_2) adj = 35% to 63%]. These discrimination diagrams represent useful binary plots to distinguish tectonic settings such as island or continental arc (Arc), continental rift (Rift), and collision (Col). This study applied the discrimination function diagrams for tectonic discrimination of siliciclastic sediments of high-silica rocks [(SiO_2)adj = 63% to 95%] to infer the tectonic setting of the Patti sandstones (Figure 12). The obtained result from discriminant function analysis present a striking support of deposition in a rift basin (Figure 12). This corroborates with the assertion made by Obaje et al. [71], that the Bida Basin is an intra-cratonic sedimentary basin. Occurence of intracratonic and rift-bounded grabens (e.g. the Benue Trough) are usually associated with a broad continental crust that is integrated in the passive-margin tectonic setting.

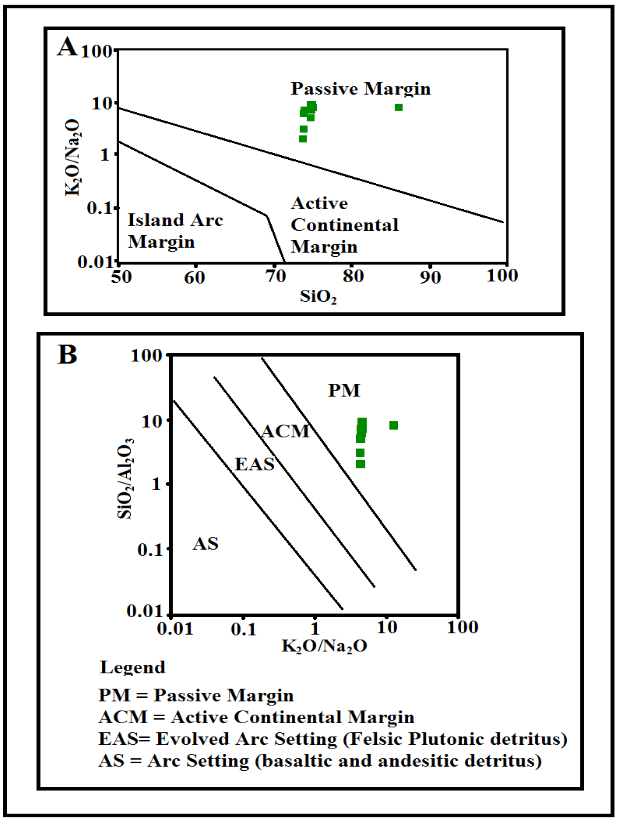

Figure 11. Bivariant paleo-tectonic discrimination plot based on: **(A)** log (K_2O/Na_2O) vs. SiO_2 and **(B)** SiO_2/Al_2O_3 Vs. K_2O/Na_2O for the investigated sandstones of Patti Formation indicating Passive Margin tectonic setting.

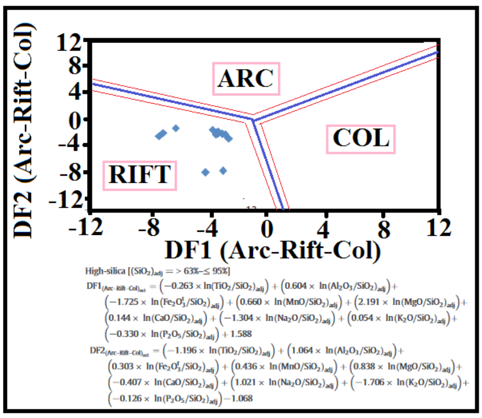

Figure 12. Tectonic discriminant diagram for the Patti sandstone, South Bida Basin. DF2 vs DF1 (arc, continental rift, and collision) (After Verma and Armstrong-Altrin [69]).

5. Conclusions

The studied sandstones from Patti Formation, Southern Bida Basin, is geochemically classified as lith-arenites, subarkose, and Fe-sands enriched in SiO_2 but low in other major oxides that signifies high mobility during processes of weathering as confirmed by high value of indices like CIA, CIW, PIA, MIA (>80) and relatively lower values obtained for the WIP (27.00 ~ 77.00), obtained values of α^{Al}_{E} with AI_2O_3-(CaO^*+Na_2O)-K_2O and CIA vs. SiO_2 indicates intense weathering in the source area. High average SiO_2 (75.41 wt%), K_2O/Na_2O ratio >1 (15.63), depleted Fe_2O_3 (1.27 wt%), Al_2O_3 (15.82 wt%), TiO_2 (0.46), enriched ΣREE (209.64 ppm), ΣLREE (195.78), LREE/HREE (27.78), negative Eu/Eu* (0.68), plots of log (K_2O/Na_2O) vs. SiO_2 and SiO_2/Al_2O_3 vs. K_2O/Na_2O with DF1 (arc-rift- col) vs. DF2 (arc-rift-col), for high-silica sediments revealed a continental rift tectonic setting. Thus, the Patti Formation sandstone underwent a high degree of weathering under a humid climatic condition within a continental rift basin that is integrated in the passive-margin tectonic setting.

Conflict of Interest

There is no conflict of interest.

References

[1] Kogbe, C.A., Ajakaiye, D.E., Matheis, G., 1983. Confirmation of Rift Structure along the Mid-Niger Valley, Nigeria. Journal of African Earth Sciences. 1, 127-131.
DOI: https://doi.org/10.1016/0899-5362(83)90004-0

[2] Udensi, E.E., Osazuwa, I.B., 2004. Spectra Determination of Depths to Magnetic Rocks under the Nupe Basin, Nigeria, 17. National Association of Petroleum Explorationist Bulletin. pp. 22-37.

[3] Odundun, O.A., Ogundoro, O.J., 2019. Origin And Sandstone Classification of the Upper Cretaceous Lokoja sandstone in Southern Bida Basin, as determined from geochemical data. Global Journal of Geological Sciences. 17, 1-11.
DOI: https://doi.org/10.4314/gjgs.v17i1.1

[4] Braide S.P., 1992. Geological development, origin and energy mineral resource potential of the Lokoja Formation in the Southern Bida Basin. Journal of Mining and Geology. 28, 33-44.

[5] Ojo, O.J., Akande, S.O., 2008. Microfloral assemblage, age and palaeovironment of the Upper Cretaceous Patti Formation, southeastern Bida Basin, Nigeria. Journal of Mining and Geology. 44, 71-81.
DOI: https://doi.org/10.4314/jmg.v44i1.18885

[6] Obaje, N.G., Wehner, H., Scheeder, G., 2004. Hydrocarbon prospectivity of Nigeria's inland basins from the viewpoint of organic geochemistry and organic petrology. American Association of Petroleum Geologists Bulletin. 88, 325-353.

[7] Jones, H.A., 1958. The Oolitic Ironstone of Agbaja Plateau, Kabba Province. Record of the Geological survey of Nigeria. 20-43.

[8] Ojo, O.J., Akande, S.O., 2013. Petrographic facies, provenance and paleo environments of the Lokoja Formation, Bida Basin, Nigeria. Journal of Mine Geology. 49, 93-110.

[9] Falconer, J.D., 1911. The Geology and Geography of Northern Nigeria. Macmillian, London pp. 255.

[10] Adeleye, D.R., 1989. The Geology of the Mid-Niger Basin. Kogbe, C. A. (Ed.), Geology of Nigeria, 2nd ed. Elizabethan Publishing Co., Lagos. pp. 283-287.

[11] Jan du Chene, R.E., Adegoke, O.S., Adediran, S.A., et al., 1978. Palynology and foraminifera of the Lokoja Sandstone (Maastrichtian), Bida Basin, Nigeria. Revista Espanola de Micropaleontotologia. 10, 379-393.

[12] Agyingi, C.M., 1991. Geology of Upper Cretaceous rocks in the eastern Bida, Nigeria. Unpublished Ph.D. Thesis. Department of Geology, University of Ibadan.

[13] Ladipo, K.O., Akande, S.O., Mucke, A., 1994. Genesis of ironstones from middle Niger sedimentary basin, evidence from sedimentological, ore microscope and geochemical studies. Journal of Mining and Geology. 30, 161-168.

[14] Abimbola, A.F., 1997. Petrographic and paragenetic studies of the Agbaja Ironstone Formation, Nupe Basin, Nigeria. Journal of African Earth Sciences. 25, 169-181.
DOI: https://doi.org/10.1016/S0899-5362(97)00096-1

[15] Akande, S.O., Ojo, O.J., Erdtmann, B.D., et al., 2005. Paleoenvironments, organic petrology and Rock-Eval studies on source rock facies of the Lower Maastrichtian Patti Formation, southern Bida Basin, Nigeria. Journal of African Earth Sciences. 41, 394-406.
DOI: https://doi.org/10.1016/j.jafrearsci.2005.07.006

[16] Nton, M.E., Adamolekun, O.J., 2016. Sedimentological and geochemical characteristics of outcrop sediments of Southern Bida Basin, Central Nigeria: Implications for provenance, paleoenvironment and tectonic history. Ife Journal of Science. 18(2), 345-369.

[17] Ojo, O.J., Adepoju, S.A., Awe, Adeoye, M.O., 2021. Mineralogy and geochemistry of the sandstone facies of Campanian Lokoja formation in the Southern Bida basin, Nigeria: implications for provenance and weathering history. Heliyon. 7, 1-12.
DOI: https://doi.org/10.1016/j.heliyon.2021.e08564

[18] Ojo, O.J., Akande, S.O., 2003. Facies relationships

and depositional environments of the Upper Cretaceous Lokoja Formation in the Bida Basin, Nigeria. Journal of Mining and Geology. 39, 39-48.
DOI: https://doi.org/10.4314/jmg.v39i1.18789

[19] Ojo, O.J., Akande, S.O., 2009. Sedimentology and depositional environments of the Maastrichtian Patti Formation, southern Bida Basin, Nigeria. Cretaceous Research. 30, 1415-1425.

[20] Bhatia, M.R., 1983. Plate tectonics and geochemical composition of sandstones. Journal of Geology. 91, 611-627.

[21] McLennan, S.M., Hemming, S., McDaniel, D.K., et al., 1993. Geochemical approaches to sedimentation, provenance, and tectonics. Processes controlling the composition of clastic sediments. Johnson, M.J and Basu, A. (Eds). Geological Society of America Special Paper. 284, 21-40.

[22] Armstrong-Altrin, J.S., Lee, Y.I., Verma, S.P., et al., 2004. Geochemistry of sandstones from the upper Miocene Kudankulam Formation, Southern India: implications for provenance, weathering, and tectonic setting. Journal of Sedimentary Research. 74(2), 285-297.
DOI: https://doi.org/10.1306/082803740285

[23] Dey, S., Rai, A.K., Chaki, A., 2009. Palaeoweathering, composition and tectonics of provenance of the Proterozoic intracratonic Kaladgi–Badami basin, Karnataka, southern India: Evidence from sandstone petrography and geochemistry. Journal of Asian Earth Sciences. 34, 703-715.
DOI: https://doi.org/10.1016/j.jseaes.2008.10.003

[24] Maharana, C., Srivastava, D., Tripathi, J.K., 2018. Geochemistry of sediments of the Peninsular Rivers of the Ganga basin and its implication to weathering, sedimentary processes, and provenance. Chemical Geology. 483, 1-20.
DOI: https://doi.org/10.1016/j.chemgeo.2018.02.019

[25] Tang, S.D.N., Atangana, J.N., Onana,V.L., 2020. Mineralogy and geochemistry of alluvial sediments from the Kadey plain, eastern Cameroon: Implications for provenance, weathering, and tectonic. setting. Journal of African Earth Sciences. 163, 103763.
DOI: https://doi.org/10.1016/j.jafrearsci.2020.103763

[26] Ayala-Perez, M.P., Armstrong-Altrin, J.S., Machain-Castillo, M.L., 2021. Heavy metal contamination and provenance of sediments recovered at the Grijalva River delta, southern Gulf of Mexico. Journal of Earth System Science. 130(880).

[27] Roser, B.P., Korsch, R.J., 1986. Determination of tectonic setting of sandstone-mudstone suites using SiO_2 content and K_2O/Na_2O ratio. Journal of Geology. 94, 635-650.

[28] Dickinson, W.R., 1985. Interpreting provenance relations from detrital modes of sandstones. Zuffa, G.G. (Ed.), Provenance of Arenites. NATO-ASI Series, 148. Reidel Publishing Company, Dordrecht. pp. 333-361.

[29] Osae, S., Asiedu, D.K., Banoeng-Yakubo, B., et al., 2006. Provenance and tectonic setting of Late Proterozoic Buem sandstones of southeastern Ghana: evidence from geochemistry and detrital modes. Journal of African Earth Sciences. 44, 85-96.

[30] Dinis, P.A., Garzanti, E., Hahn, A. et al., 2019. Weathering indices as climate proxies. A step forward based on Congo and SW African river muds. Earth Science Reviews.
DOI: https://doi.org/10.1016/j.earscirev.2019.103039

[31] Guo, Y., Yang, S., Su, N., et al., 2018. Revisiting the effects of hydrodynamic sorting and sedimentary recycling on chemical weathering indices. Geochimica et Cosmochimica Acta. 227, 48-68.
DOI: https://doi.org/10.1016/j.gca.2018.02.015

[32] Viers, J., Dupré, B., Gaillardet, J., 2009. Chemical composition of suspended sediments in World Rivers: New insights from a new database. Science of the total Environment. 407, 853-865.
DOI: https://doi.org/10.1016/j.scitotenv.2008.09.053

[33] Braide, S.P., 1992. Syntectonic fluvial sedimentation in the central Bida Basin. Journal of Mining and Geology. 28, 55-64.

[34] Petters, S.W., 1986. Depositional environments and daigenesis of Albian carbonates on the Calabar Flank, Southeastern Nigeria. Journal of Petroleum Geology. 10(3), 283-294.

[35] Ojo, O.J., Akande, S.O., 2006. Microfloral biostratigraphy, paleoecology and paleoclimate of the Upper Cretaceous Patti Formation, southeastern Bida Basin. NAPE conference Proceedings. pp. 69-73.

[36] Anaya-Gregorio, A., Armstrong-Altrin, J.S., Machain-Castillo, M.L., et al., 2018. Textural and geochemical characteristics of late Pleistocene to Holocene fine-grained deep-sea sediment cores (GM6 and GM7), recovered from southwestern, Gulf of Mexico. Journal of Palaeogeography. 7(3), 253-271.

[37] Ramos-Vazquez, M.A., Armstrong-Altrin, J.S., 2020. Sediment chemistry and detrital zircon record in the Bosque and Paseo del Mar coastal areas from the southwestern Gulf of Mexico. Marine and Petroleum Geology. 110, 650-675.
DOI: https://doi.org/10.1016/j.marpetgeo.2019.07.032

[38] Akpokodje, E.G., Etu-Efeotor, J.O., Olurunfemi, B.N., 1991. The Composition and physical properties

of some ceramic and pottery clays of South- eastern, Nigeria. Journal Mining and Geology. 27(1), 4-7.

[39] Zaid, S.M., 2017. Provenance of coastal dune sands along Red Sea, Egypt. Journal of Earth System Science. 126(4), 1-20.

[40] Bhatia, M.R., Crook, K.A.W., 1986. Trace element characteristics of greywackes and tectonic setting discrimination of sedimentary basins. Contributions to Mineralogy & Petrology. 92, 181-193. DOI: https://doi.org/10.1007/BF00375292

[41] Crichton, J.G., Condie, K.C., 1993. Trace elements as source indicators in cratonic sediments: a case of study from the early Proterozoic Libby Creek Group, southwestern Wyoming. Journal of Geology. 101, 319-322.

[42] Dabard, M.P., 1990. Lower Brioverian Formation (Upper Proterozoic) of the American Massif (France): Geodynamic evolution of source areas revealed by sandstone petrography and geochemistry. Sedimentary Geology. 69, 45-48.

[43] Taylor, S.R., McLennan, S.M., 1985. The Continental Crust: its Composition and Evolution. Blackwell Scientific Publications. pp. 312.

[44] Boynton, W.V., 1984. *G*eochemistry of the rare earth elements: meteorite studies. Henderson, P. (ed), Rare Earth Element Geochemistry, Elsevier. 63-114.

[45] Herron, M.M., 1988. Geochemical classifi cation of terrigenous sands and shales from core or log data. Journal of Sedimentary Research. 58, 820-829. DOI: https://doi.org/10.1306/212F8E77-2B24-11D7-8648000102C1865D

[46] Pettijohn, F.G., Potter, P.D., Siever, R., 1972. Sand and Sandstone. Springer, New York. pp. 618.

[47] Lindsey, D.A., Tysdal, R.G., Taggart, J.E.Jr., 2003. Chemical composition and provenance of the Mesoproterozoic Big Creek, Apple Creek, and Gunsight Formations, Lemhi Group, Central Idaho. Russell G, Tysdal RG, Lindsey DA, Taggart JE Jr, editors. Correlation, Sedimentology, Structural Setting, Chemical Composition, and Provenance of Selected Formations in Mesoproterozoic Lemhi Group, Central Idaho. Washington, DC, USA: USGS Professional Paper 1668-B.

[48] Nesbitt, H.W., Young, G.M., 1982. Early Proterozoic Climates and Plate Motions Inferred from Major Element Chemistry of Lutites. Nature. 299, 715-717.

[49] Li, C., Yang, S.Y., 2010. Is chemical index of alteration (CIA) a reliable proxy for chemical weathering in global drainage basins? American Journal of Science. 310, 111-127. DOI: https://doi.org/10.2475/02.2010.03

[50] Roy, D.K., Roser, B.P., 2013. Climatic control on the composition of Carboniferous–Permian Gondwana sediments, Khalaspir basin, Bangladesh. Gondwana Research. 2, 1163-1171. DOI: https://doi.org/10.1016/j.gr.2012.07.006

[51] Yang, J., Du, Y., Cawood, P.A., et al., 2012. Modal and geochemical compositions of the lower Silurian clastic rocks in north Qilian, NW China: Implications for provenance, chemical weathering, and tectonic setting. Journal of Sedimentary Research. 82, 92-103. DOI: https://doi.org/10.2110/jsr.2012.6

[52] Dinis, P., Garzanti, E., Vermeesch, P., et al., 2017. Climatic zonation and weathering control on sediment composition (Angola). Chemical Geology. 467, 110-121. DOI: https://doi.org/10.1016/j.chemgeo.2017.07.030

[53] Bal Akkoca, D., Eriş, K.K., Çağatay, M.N., et al., 2019. The mineralogical and geochemical composition of Holocene sediments from Lake Hazar, Elazığ, Eastern Turkey: implications for weathering, paleoclimate, redox conditions, provenance, and tectonic setting. Turkish Journal of Earth Sciences. 28, 760-785. DOI: https://doi.org/10.3906/yer-1812-8

[54] Overare, B., Osokpor, J., 2020. Providing Clues on the Paleo-weathering of Ogwashi Asaba Formation, Niger Delta Basin: Evidence from Geochemistry. Tropical Journal of Science and Technology. 1(1), 74-92.

[55] Bolarinwa, A.T., Idakwo, S.O., Bish, D.L., 2021. Source area-weathering, provenance and tectonic setting of the campanian- Maastrichtian clay sequences in the Lower Benue Trough of Nigeria. Journal of African Earth Sciences. 173, 104050. DOI: https://doi.org/10.1016/j.jafrearsci.2020.104050

[56] Condie, K.C., Boryta, M.D., Liu, J., et al., 1992. The origin of khondalites: geochemical evidence from the Archean to Early Proterozoic granulitic belt in the North China Craton: Precambrian Research. 59(3-4), 207-223.

[57] Garzanti, E., Padoan, M., Setti, M., et al., 2013. Weathering geochemistry and Sr-Nd figerprints of equatorial upper Nile and Congo muds. Geochemistry Geophysics Geosystems. 14, 292-316. DOI: https://doi.org/10.1002/ggge.20060

[58] Roy, P.D., Caballeroa, M., Lozanoc, R., et al., 2008. Geochemistry of Late quaternry sediments from Tecomulco Lake, central Mexico: Implication to chemical weathering and provenance. Chemie Der Erde Geochemistry. 68, 383-393.

[59] Nesbitt, H.W., Young, G.M., 1984. Prediction of some weathering trends of plutonic and volcanic rocks based on thermodynamic and kinetic consideration. Geochimica et Cosmochimica Acta. 48, 1523-1534.

[60] Fedo, C.M., Nesbitt, H.W., Young, G.M., 1995. Unravelling the effects of potassium metasomatism in sedimentary rocks and paleosols, with implications for paleo-weathering conditions and provenance. Geology. 23, 921-924.
DOI: https://doi.org/10.1130/0091-7613(1995)023<0921:UTEOPM>2.3.CO;2

[61] Suttner, L.J., Prodip, K.D., 1986. Alluvial sandstone composition and paleoclimate; Framework mineralogy. Journal of Sedimentary Research. 56(3), 329-345.
DOI: https://doi.org/10.1306/212F8909-2B24-11D7-8648000102C1865D

[62] Wronkiewicz, D.J., Condie, K.C., 1987. Geochemistry of Archean shales from the Witwatersrand Supergroup, South Africa: Source area weathering and provenance. Geochimica et Cosmochimica Acta. 51, 2401-2416.
DOI: https://doi.org/10.1016/0016-7037(87)90293-6

[63] Tang, Y., Sang, L., Yuan, Y., et al., 2012. Geochemistry of Late Triassic pelitic rocks in the NE part of Songpan-Ganzi Basin, western China: implications for source weathering, provenance and tectonic setting. Geoscience Frontiers. 3(5), 647-660.
DOI: https://doi.org/10.1016/j.gsf.2012.01.006

[64] Mourabet, M., Barakat, A., Zaghloul, M.N., et al., 2018. Geochemistry of the Miocene Zoumi flysch thrust-top basin (External Rif, Morocco): new constraints on source area weathering, recycling processes, and paleoclimate conditions. Arabian Journal of Geosciences. 11(6), 18-26.
DOI: https://doi.org/10.1007/s12517-018-3465-y

[65] McLennan, S.M., Taylor, S.R., McCulloch, M.T., et al., 1990. Geochemical and Nd–Sr isotopic composition of deep-sea turbidites: crustal evolution and plate tectonic associations. Geochimica et Cosmochimica Acta. 54, 2015-2050.
DOI: https://doi.org/10.1016/0016-7037(90)90269-Q

[66] Armstrong-Altrin, J.S., Machain-Castillo, M.L., Rosales-Hoz, L., et al., 2015. Provenance and depositional history of continental slope sediments in the southwestern Gulf of Mexico unraveled by geochemical analysis. Continental Shelf Research. 95, 15-26.
DOI: https://doi.org/10.1016/j.csr.2015.01.003

[67] McLennan, S.M., Taylor, S.R., 1991. Sedimentary rocks and crustal evolution: Tectonic setting and secular trends. Journal of Geology. 99, 1-21.

[68] LaMaskin, T.A., Dorsey, R., Vervoort, J.D., 2008. Tectonic controls on mudrock geochemistry, Mesozoic rocks of eastern Oregon and western Idaho, USA: implications for Cordilleran tectonics. Journal of Sedimentary Research. 78(12), 765-783.
DOI: https://doi.org/10.2110/jsr.2008.087

[69] Verma, S.P., Armstrong-Altrin, J.S., 2013. New multi-dimensional diagrams for tectonic discrimination of siliciclastic sediments and their application to Precambrian basins. Chemical Geology. 355, 117-180.
DOI: https://doi.org/10.1016/j.chemgeo.2013.07.014

[70] Armstrong-Altrin, J.S., Botello, A.V., Villanueva, S.F., et al., 2019. Geochemistry of surface sediments from the north western Gulf of Mexico: implications for provenance and heavy metal contamination. Geological Quarterly. 63(3), 522-538.
DOI: https://doi.org/10.7306/gq.1484

[71] Obaje, N.G., Balogun, D.O., Idris-Nda, A., et al., 2013. Preliminary integrated hydrocarbon prospectivity evaluation of the Bida Basin in North Central Nigeria. Petroleum Technology Development Journal. 3(2), 36-65.